Available online at www.sciencedirect.com
SCIENCE DIRECT
Journal of Catalysis 233 (2005) 210–220
JOURNAL OF CATALYSIS
www.elsevier.com/locate/jcat

# The effects of zirconia morphology on methanol synthesis from CO and $H_2$ over $Cu/ZrO_2$ catalysts Part II. Transient-response infrared studies

Michael D. Rhodes, Konstantin A. Pokrovski, Alexis T. Bell *

*Chemical Sciences Division, Lawrence Berkeley National Laboratory, and Department of Chemical Engineering, University of California, Berkeley, CA 94720-1462, USA*

Received 31 December 2004; revised 23 March 2005; accepted 24 April 2005

Available online 31 May 2005

**Abstract**

The interactions of CO, $CO/H_2$, $H_2$, $D_2$, and $CH_3OH$ with t-$ZrO_2$, m-$ZrO_2$, Cu/t-$ZrO_2$, and Cu/m-$ZrO_2$ were investigated by in situ infrared spectroscopy with the aim of understanding the nature of species involved in methanol synthesis and the dynamics of the formation and consumption of these species. With both phases of $ZrO_2$, the primary surface species observed during CO hydrogenation were bidentate formate groups, b-HCOO–Zr, and methoxide groups, $CH_3O$–Zr. Transient-response experiments indicated that the rate-limiting step for each catalyst is the reductive elimination of methoxide species. Relative to 1.2 wt% Cu/t-$ZrO_2$, however, spillover of H atoms and the formation and reduction of formate and methoxide species proceeded more rapidly on the more active 1.2 wt% Cu/m-$ZrO_2$. Steady-state intensities of surface species were also larger on 1.2 wt% Cu/m-$ZrO_2$. These differences are attributed to the higher reactivity of the hydroxyl groups on the surface of m-$ZrO_2$. Increasing the Cu surface area on m-$ZrO_2$ increases the rate of reductive elimination of methoxide species up to a maximum value, determined by the eventual saturation of the $ZrO_2$ surface with H atoms via spillover from Cu. The product of the apparent rate coefficient for reductive elimination of methoxide species and the surface concentration of these species increases linearly with increasing Cu surface area, which is consistent with the proportionality seen in the rate of methanol synthesis at steady state.


*Keywords:* Methanol synthesis; Infrared spectroscopy; Cu; $ZrO_2$; $H_2$; CO

## 1. Introduction

Cu supported on $ZrO_2$ with Cu is a very active catalyst for the synthesis of methanol from CO and $H_2$ [1–12]. Previous studies have shown that both catalyst components play a role in the hydrogenation of CO to methanol: $ZrO_2$ adsorbs CO and all carbon-containing intermediates, leading to methanol, whereas supported Cu particles adsorb $H_2$, and then H atoms spill over onto the surface of $ZrO_2$, where they participate in the hydrogenation of CO. In Part I of the present study we demonstrated that the phase of $ZrO_2$ has a strong influence on catalyst activity and selectivity [13]. Catalysts prepared with monoclinic $ZrO_2$ (m-$ZrO_2$) are nearly an order of magnitude more active for methanol synthesis activities and exhibit higher methanol selectivities than catalysts with the same Cu surface density deposited on tetragonal $ZrO_2$ (t-$ZrO_2$) with the same surface area as m-$ZrO_2$. These differences are attributed to the higher concentration of anionic defects on m-$ZrO_2$ than t-$ZrO_2$. Such defects, when present adjacent to surface hydroxyl groups, readily adsorb CO to form bidentate formate groups. It was also shown that the methanol synthesis activity of $Cu/ZrO_2$ is proportional to the surface area of the deposited Cu. Increasing the overall Cu surface area increases the rate of H atom spillover and, hence, the rate of hydrogenation of adsorbed CO to methanol.

* Corresponding author.
*E-mail address:* bell@cchem.berkeley.edu (A.T. Bell).

0021-9517/$ – see front matter 
doi:10.1016/j.jcat.2005.04.027

In Part II of this study, in situ FTIR spectroscopy was used to investigate the dynamics of CO adsorption and CO hydrogenation on Cu/m-$ZrO_2$ and Cu/t-$ZrO_2$ at reaction temperature. This work was undertaken to determine the nature of the adsorbed species formed and their relationship to the mechanism of methanol synthesis. These transient-response studies also provided insights into relative rates at which elementary processes occur on Cu/m-$ZrO_2$ and Cu/t-$ZrO_2$. The effects of the concentration of exposed Cu atoms on the dynamics of CO hydrogenation were also investigated.

## 2. Experimental

The preparation and characterization of the Cu/$ZrO_2$ catalysts used in this study have been described previously [13]. Both t-$ZrO_2$ and m-$ZrO_2$ have a surface area of $\sim 145\ m^2/g$. Cu was deposited on each support by deposition-precipitation, which was found to yield a higher dispersion of Cu compared with incipient-wetness impregnation [14]. The surface areas of the dispersed Cu were determined by $H_2$-TPR after $N_2O$ titration [14]; the results are presented in Table 1.

The steady-state methanol synthesis activity of each sample was measured with a glass-lined microreactor. A 3:1 mixture of $H_2$ and CO was supplied to the reactor from a gas manifold, and the reaction products were analyzed by gas chromatography. A more detailed description of the reactor apparatus is given in Ref. [13]. Steady-state rate data were collected at 523 K, a total pressure of 3.0 MPa, and a feed flow rate of 60 $cm^3/min$.

In situ transmission infrared spectroscopy experiments were conducted with a low-dead-volume infrared cell equipped with $CaF_2$ windows [15]. Samples were pressed into pellets with a density of approximately 0.015 $g/cm^3$. Infrared spectra were collected with a Nicolet Magna 750 series II FTIR spectrometer equipped with a narrow-band MCT detector. We obtained in situ absorbance spectra collecting either 32 or 128 scans at 2 $cm^{-1}$ resolution, which were then referenced to a spectrum of the catalyst taken after pretreatment in flowing He at the same temperature as that used for reaction. The cell was heated by electrical resistance heaters, controlled by a programmable temperature controller (Omega), and the sample temperature was monitored by a thermocouple located just above the catalyst pellet inside the cell.

Table 1
Surface area and methanol synthesis activity for Cu/t-$ZrO_2$ and Cu/m-$ZrO_2$[a]

| Sample | Cu surface area ($m^2/g$) | Mass specific rate ($\mu mol/(g_{cat}\ s)$) |
|---|---|---|
| 1.2 wt% Cu/t-$ZrO_2$ | 1.44 | 0.14 |
| 1.2 wt% Cu/m-$ZrO_2$ | 0.87 | 1.1 |
| 6.4 wt% Cu/m-$ZrO_2$ | 2.46 | 2.7 |
| 10 wt % Cu/m-$ZrO_2$ | 2.70 | 3.0 |
| 20 wt% Cu/m-$ZrO_2$ | 1.88 | 1.5 |

[a] Reaction conditions: $T = 523$ K; $P = 3.0$ MPa; $H_2/CO = 3$; total flow rate = 60 $cm^3/min$.

The reactants used for the infrared experiments were purified before delivery to the sample cell. $H_2$ (99.999%) (Airgas) was purified with the use of Oxi-Clear (Alltech) traps to remove $O_2$ and $H_2O$. He (99.999%) was passed through a synthetic zeolite adsorbent (Alltech) to remove CO, $CO_2$, $O_2$, and $H_2O$ impurities. Another molecular sieve trap (Alltech) was used to remove $CO_2$ and $H_2O$ from 15% CO/He (99.99%) (Airgas). The purified gases were delivered to the infrared cell with Tylan mass flow controllers. A stream of 0.5% $CH_3OH$/He (99%) was delivered with a needle valve without further purification. Pressure in the cell was controlled with a back-pressure regulator (Go).

To remove any residual surface species before testing, each sample was calcined in a 10% $O_2$/He mixture flowing at 60 $cm^3/min$. The sample was heated from room temperature to 523 K at 2 K/min and then maintained at 523 K for 8 h. Next, the sample was cooled to 323 K, swept with He, and reduced in a 10% $H_2$/He mixture flowing at a rate of 60 $cm^3/min$ while the temperature was increased at a rate of 2 K/min to 523 K. The flow of 10% $H_2$/He was maintained at 523 K for 1 h before the flow was switched to 100% $H_2$ for an additional 1–3 h. The sample was then flushed with He for 1 h before the initiation of an experiment.

## 3. Results

### 3.1. 1.2 wt% Cu/t-$ZrO_2$

Fig. 1 shows infrared spectra obtained during CO adsorption at 523 K on 1.2 wt% Cu/t-$ZrO_2$ exposed to a flow of 15% CO/He at a total pressure of 0.50 MPa. Strong bands are observed at 1567, 1385, and 1367 $cm^{-1}$, which are attributable to the $\upsilon_{as}$(OCO), $\delta$(CH), and $\upsilon_s$(OCO) modes, respectively, of b-HCOO–Zr [9,16–23]. In the C–H stretching region, features at 2973 and 2892 $cm^{-1}$ become apparent after about 15 min and grow in intensity with time. The 2892 $cm^{-1}$ band is assigned to the C–H stretching vibration of b-HCOO–Zr [9,16–22,25], and the 2973 $cm^{-1}$ band is attributed to a combination of the asymmetric O–C–O stretching and C–H bending modes of the same species [20,21,24,25]. Virtually identical spectra were obtained upon exposure of t-$ZrO_2$ in the absence of Cu, confirming that Cu does not influence the adsorption of CO as bidentate formate species on the surface of t-$ZrO_2$.

Formate formation has been attributed to the interaction of CO with hydroxyl groups on $ZrO_2$ during CO adsorption [18,26–29]. Evidence for this interaction is presented in Fig. 2, which shows spectra obtained in the OH stretching region during the experiment presented in Fig. 1. Bands appear at 3660 and 3738 $cm^{-1}$ which are due to Zr–OH groups on t-$ZrO_2$ [30,31]. These bands are negative and increase in intensity with the duration of CO exposure, indicating that ZrOH groups are consumed upon the adsorption of CO.

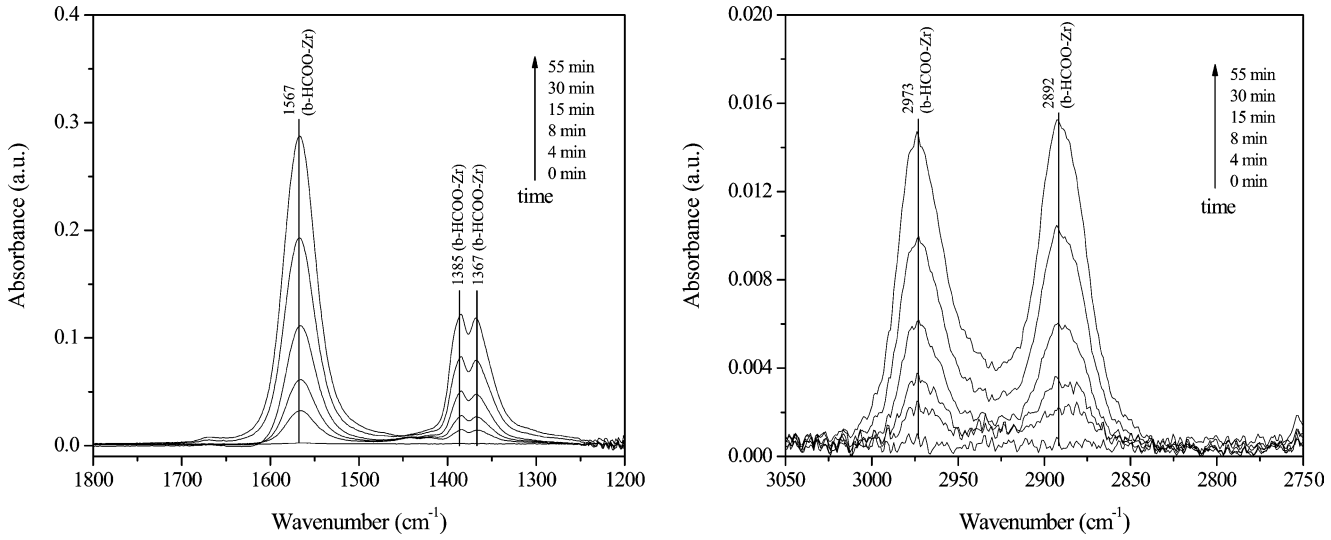


Fig. 1. Infrared spectra (C–H and C–O stretching regions) taken for 1.2 wt% Cu/t-$ZrO_2$ at 523 K after switching feed from 0.50 MPa He to 0.05 MPa CO and 0.45 MPa He flowing at a total rate of 60 $cm^3$/min. Spectra referenced to 1.2 wt% Cu/t-$ZrO_2$ under 0.50 MPa He flow at 523 K.

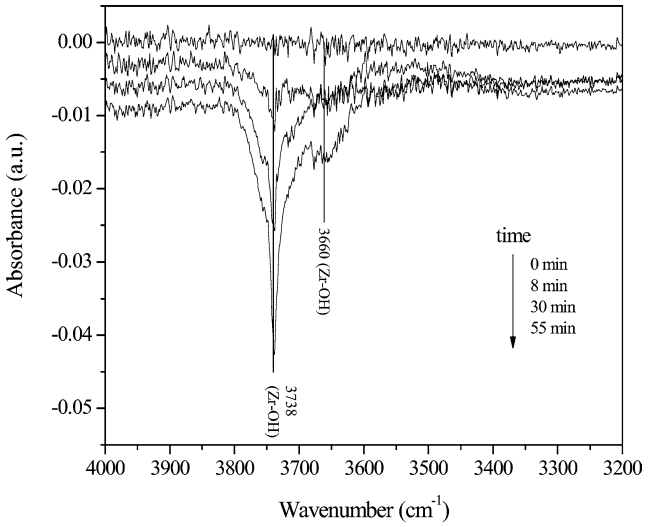


Fig. 2. Infrared spectra (O–H stretching region) taken for 1.2 wt% Cu/t-$ZrO_2$ at 523 K after switching feed from 0.50 MPa He to 0.05 MPa CO and 0.45 MPa He flowing at a total rate of 60 $cm^3$/min. Spectra referenced to 1.2 wt% Cu/t-$ZrO_2$ under 0.50 MPa He flow at 523 K.

After CO adsorption for 1 h, transient-response spectra were recorded during CO hydrogenation at 523 K. $H_2$ was introduced into the flowing 15% CO/He (total pressure = 0.50 MPa) so as to achieve a $H_2$/CO ratio of 3:1. Fig. 3 shows that the features for b-HCOO–Zr (2973, 2894, 1565, 1384, and 1366 $cm^{-1}$) continue to increase in intensity up to about 4 h, at which time they approach a steady-state level. After about 4 min, bands at 2937 and 2837 $cm^{-1}$, attributable to the $\upsilon(CH_3)$ modes of $CH_3O$–Zr [17,18,20,26,30,32,34], become apparent. These bands increase in intensity, reaching a steady-state level after approximately 4 h. A small band at approximately 1474 $cm^{-1}$ becomes apparent at longer times and is ascribed to the $\delta(CH)$ mode of $CH_3O$–Zr species [9,21,33].

### 3.2. 1.2 wt% Cu/m-$ZrO_2$

Fig. 4 shows infrared spectra recorded during CO adsorption on 1.2 wt% Cu/m-$ZrO_2$ at 523 K. The catalyst was exposed to a flow of 15% CO/He at a total pressure of 0.50 MPa. The features for b-HCOO–Zr (2969, 2883, 2748, 1563, 1386, and 1366 $cm^{-1}$) are significantly more intense than the analogous bands observed for 1.2 wt% Cu/t-$ZrO_2$. The small band in the C–H stretching region at 2745 $cm^{-1}$ is ascribed to a combination of the $\delta(CH)$ and $\upsilon_s(OCO)$ modes of b-HCOO–Zr [21,24]. Features attributable to $CH_3O$–Zr (2934 and 2830 $cm^{-1}$) appear almost immediately, even in the absence of gas-phase $H_2$, and continue to increase in intensity for the duration of the experiment ($\sim$ 1 h). At the same time, bands appear at 1039 and 1142 $cm^{-1}$ and increase in intensity at a rate similar to that for the bands at 2936 and 2836 $cm^{-1}$. These peaks are assigned, respectively, to the C–O stretch of terminal (t-$OCH_3$) and bridged (b-$OCH_3$) methoxide species on $ZrO_2$ [33,35,36]. The features at 1034 and 1142 $cm^{-1}$ were not observable with 1.2 wt% Cu/t-$ZrO_2$ because of strong sample absorptions below 1200 $cm^{-1}$. The shoulder located at approximately 1320 $cm^{-1}$ is assigned to b-$CO_3^{2-}$–Zr species [23,26]. Similar spectra were recorded for m-$ZrO_2$ in the absence of Cu. The primary difference is that the intensity of the bands for formate species in the spectra for 1.2 wt% Cu/m-$ZrO_2$ are less intense than those observed on m-$ZrO_2$, possibly because of the hydrogenation of some of these species to methoxy groups in the former case. However, as with 1.2% Cu/t-$ZrO_2$, all of the bands observed during the adsorption of CO on 1.2% Cu/m-$ZrO_2$ are ascribable to adsorption on $ZrO_2$.

Fig. 5 presents spectra obtained in the OH stretching region during the adsorption of CO on 1.2% Cu/m-$ZrO_2$. Negative absorbance bands at 3730 and 3670 $cm^{-1}$ are ascribed to the consumption of Zr–OH groups on m-$ZrO_2$ [30,31].

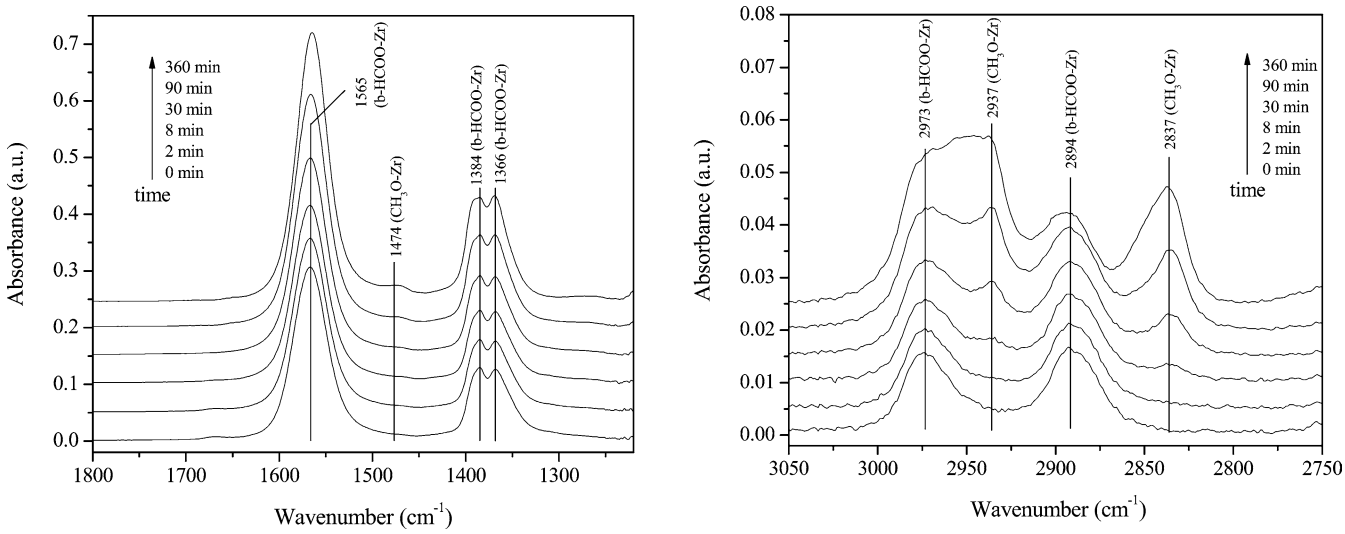


Fig. 3. Infrared spectra taken for 1.2 wt% Cu/t-$ZrO_2$ at 523 K after switching feed from 0.05 MPa CO and 0.45 MPa He to 0.05 MPa CO, 0.15 MPa $H_2$, and 0.30 MPa He flowing at a total rate of 60 $cm^3$/min. Spectra referenced to 1.2 wt% Cu/t-$ZrO_2$ under 0.50 MPa He flow at 523 K.

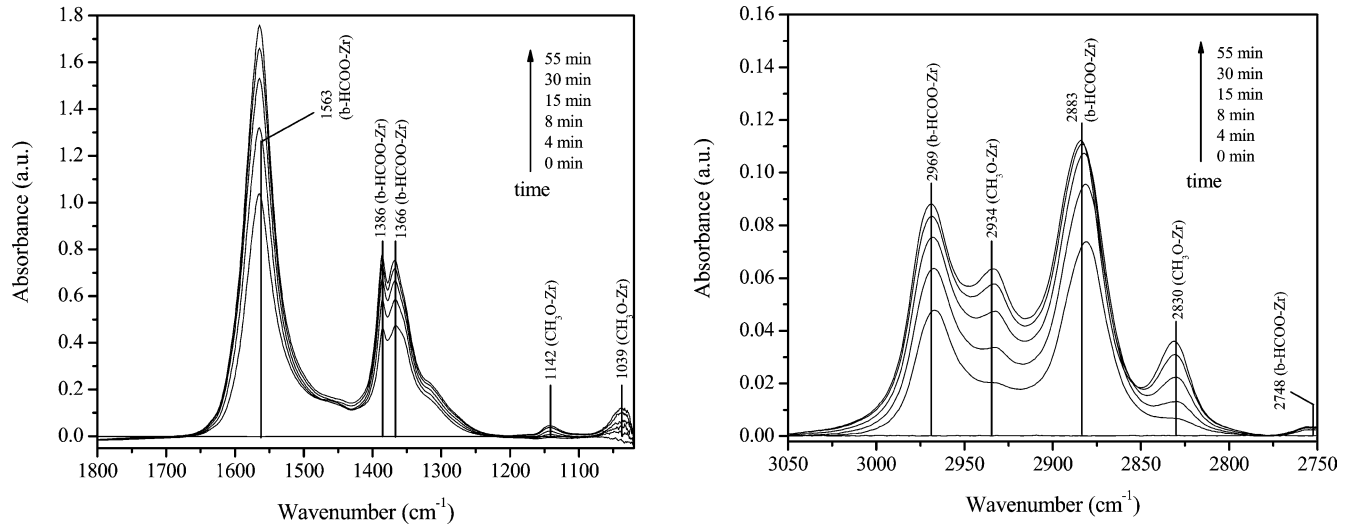


Fig. 4. Infrared spectra (C–H and C–O stretching regions) taken for 1.2 wt% Cu/m-$ZrO_2$ at 523 K after switching feed from 0.50 MPa He to 0.05 MPa CO and 0.45 MPa He flowing at a total rate of 60 $cm^3$/min. Spectra referenced to 1.2 wt% Cu/m-$ZrO_2$ under 0.50 MPa He flow at 523 K.

Consistent with the larger amount of formate species detected on 1.2 wt% Cu/m-$ZrO_2$, a significantly greater decrease in Zr–OH was observed compared with that seen during CO adsorption on 1.2 wt% Cu/t-$ZrO_2$ (Fig. 2). Cu/m-$ZrO_2$ at 1.2 wt% exhibits a larger consumption of lower-frequency hydroxyl species relative to the higher-frequency hydroxyl species, which is the opposite of what is observed on 1.2 wt% Cu/t-$ZrO_2$. This observation suggests that the Zr–OH groups responsible for the band at 3670 $cm^{-1}$ are consumed by reaction with CO more slowly than those at 3730 $cm^{-1}$.

Fig. 6 shows transient-response spectra obtained during CO hydrogenation on 1.2 wt% Cu/m-$ZrO_2$ at 523 K. We obtained spectra by introducing $H_2$ into the flowing 15% CO/He (total pressure = 0.50 MPa) so as to achieve a $H_2$/CO ratio of 3:1. The features for b-HCOO–Zr at 1564, 1385, and 1367 $cm^{-1}$ rapidly decrease in intensity as soon as $H_2$ is introduced, while, concurrently, peaks for $CH_3O$–Zr at 1039 and 1142 $cm^{-1}$ rapidly increase in intensity. In the C–H stretching region, the bands for $CH_3O$–Zr are particularly intense and increase in intensity until they reach a steady-state level after approximately 80 min. The corresponding C–O stretching bands (1039 and 1142 $cm^{-1}$) increase in a similar manner. As adsorption progresses, each C–H stretch red shifts by approximately 10–15 $cm^{-1}$, and each of the C–O stretches blue shifts by approximately 3–8 $cm^{-1}$, possibly because of interactions between surface species as surface coverage increases. The $\delta$(CH) feature for $CH_3O$–Zr (1446 $cm^{-1}$) is evident initially but remains relatively small throughout the transient. A comparison of Figs. 4 and 6 shows that the intensities of the bands for $CH_3O$–Zr are ap-

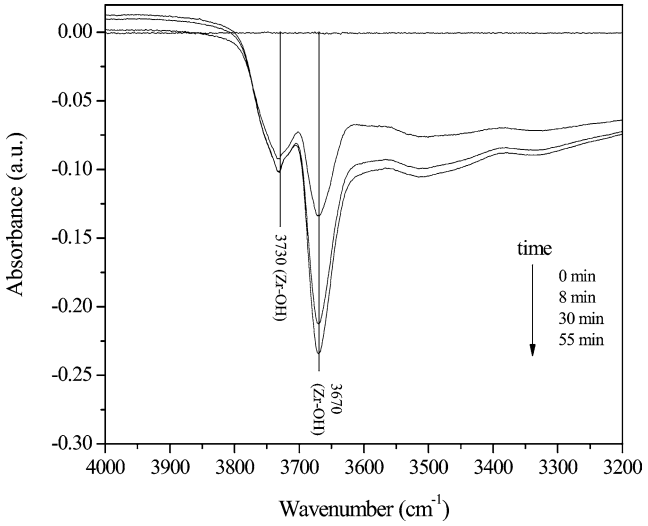


Fig. 5. Infrared spectra (O–H stretching region) taken for 1.2 wt% Cu/m-$ZrO_2$ at 523 K after switching feed from 0.50 MPa He to 0.05 MPa CO and 0.45 MPa He flowing at a total rate of 60 $cm^3$/min. Spectra referenced to 1.2 wt% Cu/m-$ZrO_2$ under 0.50 MPa He flow at 523 K.

proximately an order of magnitude larger on 1.2 wt% Cu/m-$ZrO_2$ than on 1.2 wt% Cu/t-$ZrO_2$.

### 3.3. Transient-response experiments

The temporal evolution of the principal surface species on 1.2% Cu/t-$ZrO_2$ and that on 1.2% Cu/m-$ZrO_2$ during the CO hydrogenation are compared in Fig. 7. The band at 1564(5) $cm^{-1}$ was used to follow the dynamics of b-HCOO–Zr, and the band at either 2837 or 2821 $cm^{-1}$ was used to follow the dynamics of $CH_3O$–Zr. The peak areas for b-HCOO–Zr and $CH_3O$–Zr were normalized to the value observed after approximately 12 h of exposure to $CO/H_2$. For 1.2 wt% Cu/t-$ZrO_2$ the concentration of b-HCOO–Zr continues to rise after 1 h of CO adsorption (represented by time 0 in Fig. 7). In contrast, the concentration of formate species on 1.2 wt% Cu/m-$ZrO_2$ undergoes a rapid initial decrease relative to the level observed in the absence of gas-phase $H_2$, before decreasing more slowly over the remainder of the transient.

The intensity of the band for $CH_3O$–Zr increases with the time of catalyst exposure to the $CO/H_2$ mixture, but the dynamics of band growth are quite different for 1.2% Cu/t-$ZrO_2$ and 1.2% Cu/m-$ZrO_2$. For 1.2 wt% Cu/m-$ZrO_2$ the intensity of the $CH_3O$–Zr band increases very rapidly over the initial 25 min and then approaches a plateau after about 1 h. The dynamics of this feature are very similar to those for the band associated with b-HCOO–Zr, but opposite in direction, suggesting that on 1.2% Cu/m-$ZrO_2$, b-HCOO–Zr undergoes rapid hydrogenation to $CH_3O$–Zr. In contrast, the intensity of the HCOO–Zr band on 1.2 wt% Cu/t-$ZrO_2$ increases with time, suggesting a slower conversion of formate to methoxide species.

We probed the rate at which surface species are consumed by removing CO from the feed at the conclusion of the CO hydrogenation experiments shown in Figs. 3 and 6. Fig. 8 compares the dynamics of b-HCOO–Zr and $CH_3O$–Zr consumption on 1.2% Cu/t-$ZrO_2$ and 1.2% Cu/m-$ZrO_2$. We obtained transient-response spectra by replacing the flow of 15% CO/He in the flow used for CO hydrogenation with an equivalent flow of pure He, while maintaining a constant $H_2$ partial pressure of 0.15 MPa. The intensity of the band for b-HCOO–Zr decreased monotonically for both catalysts, but much more rapidly for 1.2% Cu/m-$ZrO_2$. The intensity of the band for $CH_3O$–Zr also underwent a monotonic decrease for both catalysts, but the rate of decrease was significantly slower than that for b-HCOO–Zr. Fig. 8c shows that immediately upon cessation of the flow of CO, there was a short period during which the surface concentration of $CH_3O$–Zr remained relatively constant before it began to decline. This observation suggests that formate species undergo rapid hy-

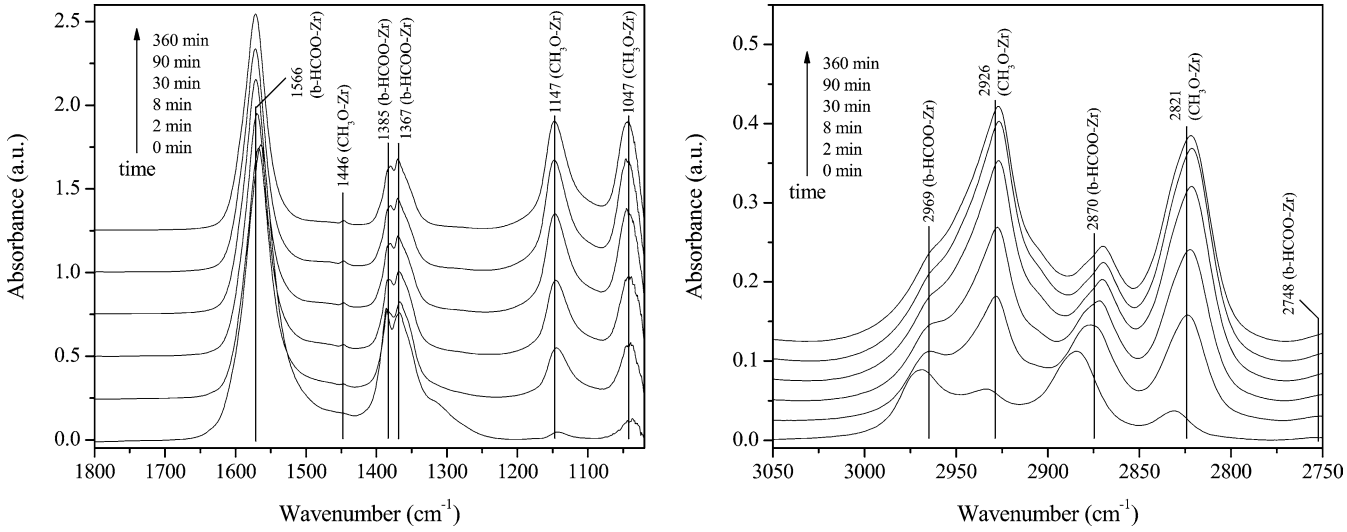


Fig. 6. Infrared spectra taken for 1.2 wt% Cu/m-$ZrO_2$ at 523 K after switching feed from 0.05 MPa CO and 0.45 MPa He to 0.05 MPa CO, 0.15 MPa $H_2$, and 0.30 MPa He flowing at a total rate of 60 $cm^3$/min. Spectra referenced to 1.2 wt% Cu/m-$ZrO_2$ under 0.50 MPa He flow at 523 K.

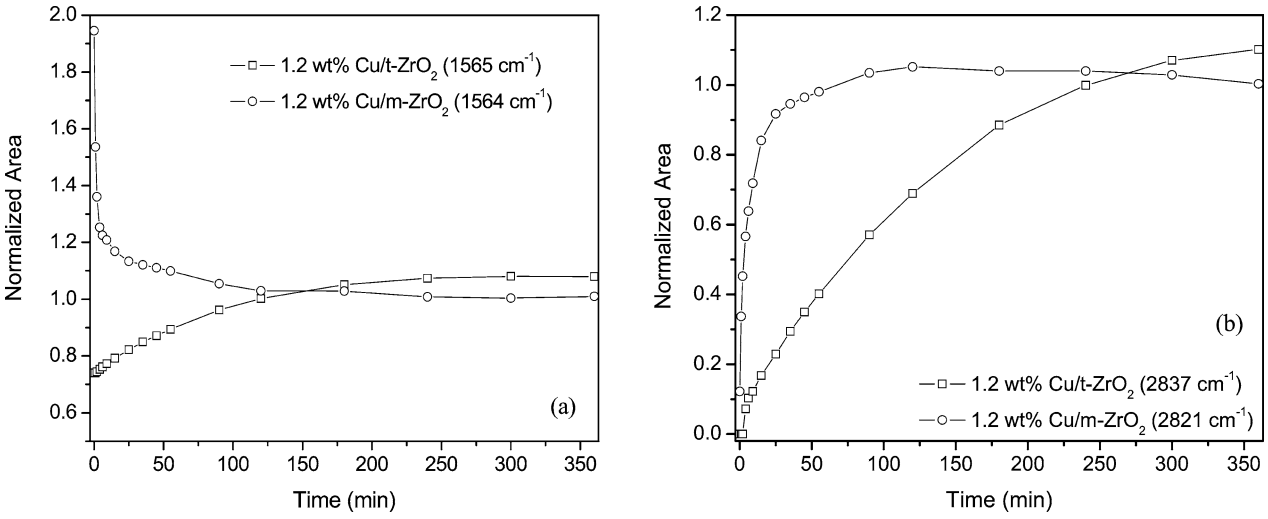


Fig. 7. Relative IR peak intensities versus time for (a) b-HCOO–Zr and (b) $CH_3O$–Zr observed for 1.2 wt% Cu/t-$ZrO_2$ and 1.2 wt% Cu/m-$ZrO_2$ during the experiments shown in Figs. 3 and 6. Areas normalized to the values observed at the end of the transient.

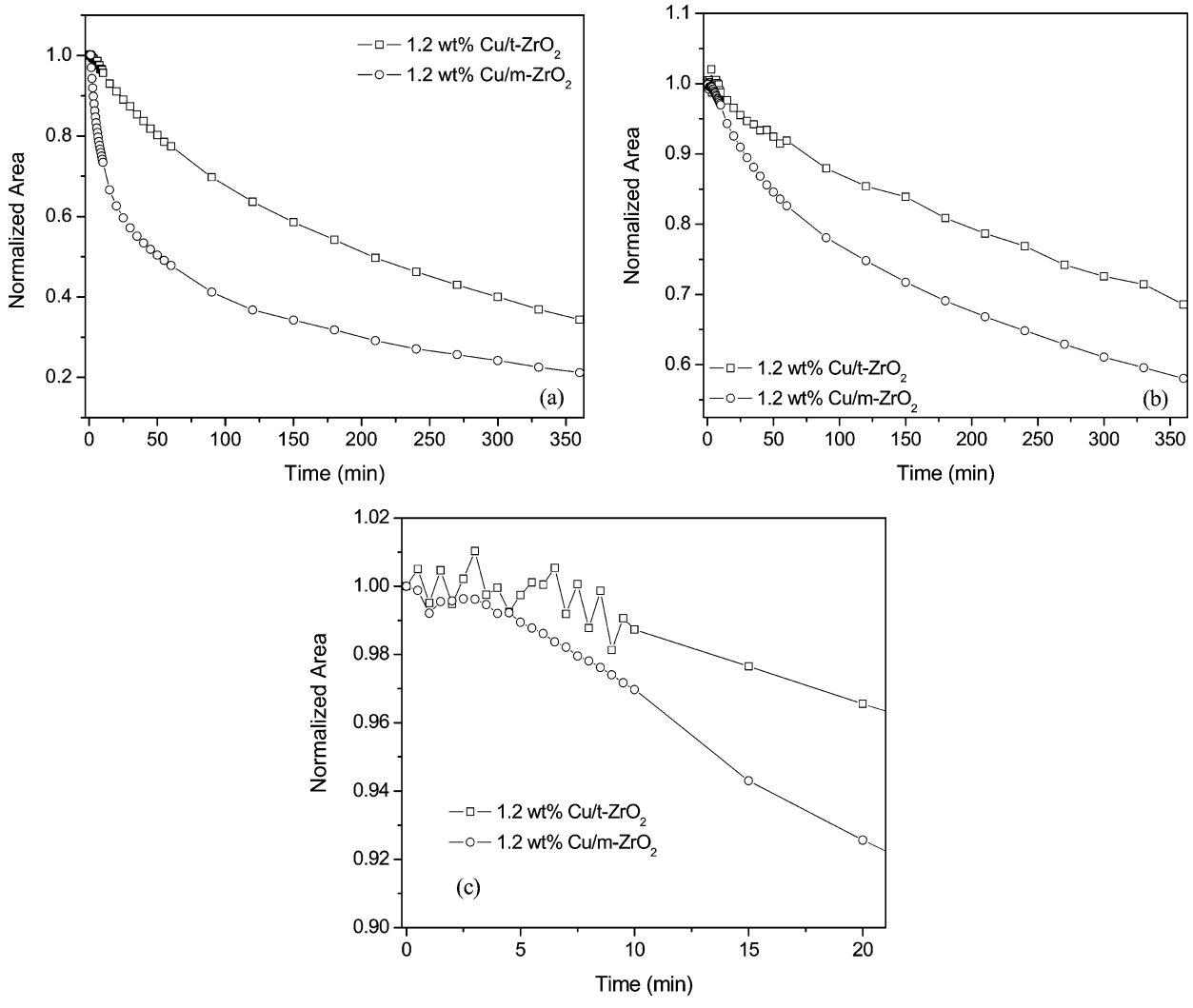


Fig. 8. Relative IR peak intensities versus time for (a) b-HCOO–Zr, (b) $CH_3O$–Zr, and (c) initial 20 min of (b) observed for 1.2 wt% Cu/t-$ZrO_2$, and 1.2 wt% Cu/m-$ZrO_2$ at 523 K after switching feed from 0.05 MPa CO, 0.15 MPa $H_2$, and 0.30 MPa He to 0.15 MPa $H_2$ and 0.35 MPa He flowing at a total rate of 60 $cm^3$/min. Areas normalized to the values observed at the beginning of the transient.

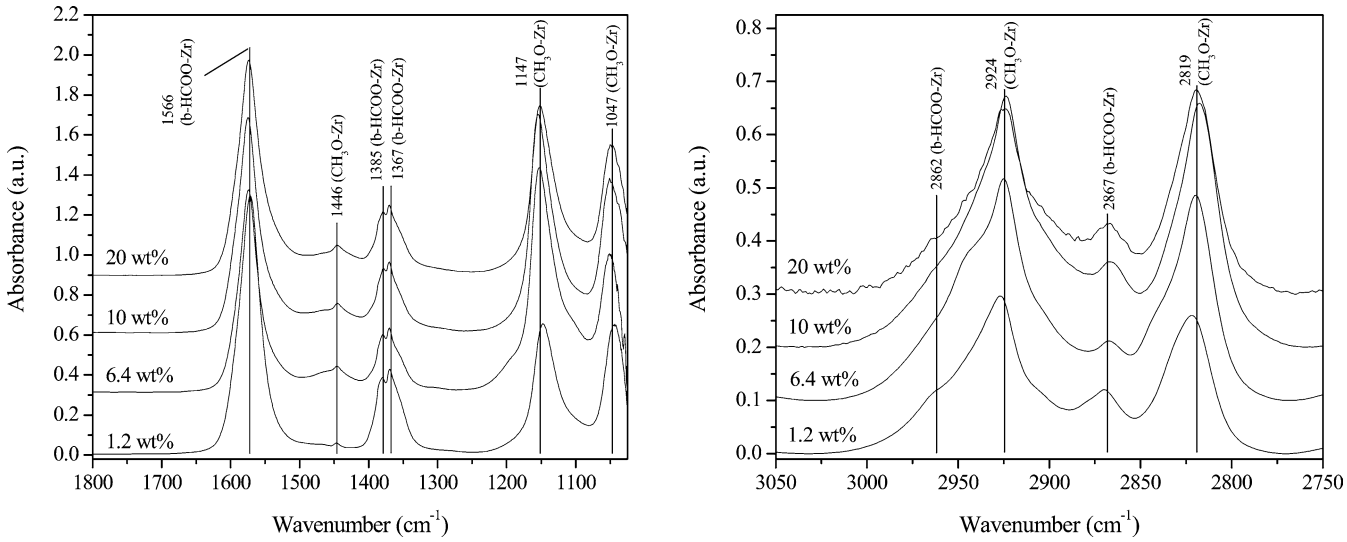


Fig. 9. Infrared spectra taken for 1.2, 6.4, 10, and 20 wt% Cu/m-$ZrO_2$ at 523 K after switching feed from 0.05 MPa CO to 0.45 MPa He to 0.05 MPa CO, 0.15 MPa $H_2$, and 0.30 MPa He flowing at a total rate of 60 $cm^3$/min. Spectra referenced to 1.2, 6.4, 10, and 20 wt% Cu/m-$ZrO_2$ under 0.50 MPa He flow at 523 K, respectively.

drogenation to methoxide species on both phases of $ZrO_2$, but that the reductive elimination of methoxide species occurs at a slower rate. Figs. 8b and 8c show that the rate of removal of $CH_3O$–Zr was initially more rapid on 1.2% Cu/m-$ZrO_2$ than on 1.2% Cu/t-$ZrO_2$, but that for longer times the relative rates became comparable.

### 3.4. Effect of Cu loading on Cu/m-$ZrO_2$

The results presented in Part I of this study demonstrated that Cu/m-$ZrO_2$ exhibits a higher steady-state methanol synthesis activity than Cu/t-$ZrO_2$ (see Table 1). Increasing the Cu surface density on m-$ZrO_2$ further improves the activity. Experiments were carried out to investigate the effects of Cu loading on the dynamics of species formation and consumption. Fig. 9 shows spectra for Cu/m-$ZrO_2$ catalysts taken after 6 h of CO hydrogenation at 523 K with a 3:1 $H_2$/CO ratio and a total pressure of 0.50 MPa. Comparison of these spectra reveals that although the intensity of the bands for b-HCOO–Zr are relatively independent of Cu loading and Cu surface coverage, the intensity of the bands for $CH_3O$–Zr increases with Cu surface coverage (Table 2).

A comparison of the temporal evolution of b-HCOO–Zr and $CH_3O$–Zr during the onset of CO hydrogenation after CO adsorption for 1 h over each catalyst is presented in Fig. 10. Peak areas for both b-HCOO–Zr and $CH_3O$–Zr have been normalized to the value observed after reaction for approximately 12 h. The dynamics of b-HCOO–Zr consumption are independent of Cu loading. Initially, the surface concentration of b-HCOO–Zr decreases rapidly from the level observed before the introduction of $H_2$, after which it declines more slowly over the remainder of the transient. Although the absolute concentration of $CH_3O$–Zr varies among Cu/m-$ZrO_2$ catalysts, the relative dynamics of $CH_3O$–Zr formation are also virtually independent of Cu loading. The time scale of the rise in the concentration of $CH_3O$–Zr closely parallels the pattern of decrease in the surface concentration of b-HCOO–Zr.

Table 2
Steady-state peak areas of $CH_3O$–Zr and apparent first-order rate coefficients for the removal of $CH_3O$–Zr from 1.2, 6.4, 10, and 20 wt% Cu/m-$ZrO_2$

| Sample | $k_{app}$ ($min^{-1}$) | $\theta_{CH_3O}$ (a.u.) |
|---|---|---|
| 1.2 wt% Cu/m-$ZrO_2$ | $4.1 \times 10^{-3}$ | 12.9 |
| 6.4 wt% Cu/m-$ZrO_2$ | $8.2 \times 10^{-3}$ | 21.3 |
| 10 wt% Cu/m-$ZrO_2$ | $7.7 \times 10^{-3}$ | 21.6 |
| 20 wt% Cu/m-$ZrO_2$ | $7.6 \times 10^{-3}$ | 16.5 |

We examined the relative rate of consumption of surface species by replacing the flow of CO used for CO hydrogenation with an equivalent flow of He while maintaining the $H_2$ partial pressure. Fig. 11 compares the dynamics of b-HCOO–Zr and $CH_3O$–Zr consumption for each of the Cu/m-$ZrO_2$ catalysts. Peak areas for both b-HCOO–Zr and $CH_3O$–Zr are normalized to the value observed at the beginning of the transient. The initial rate of consumption of b-HCOO–Zr is independent of Cu loading. After approximately 20 min, however, the rate of b-HCOO–Zr consumption from the higher weight-loaded materials decreases significantly. This suggests the possible existence of two distinct formate species present on the surface of m-$ZrO_2$. A similar distinction has been reported with formate species formed on ZnO in studies of CO hydrogenation on Cu/ZnO/$Al_2O_3$ [37]. In contrast to the removal of b-HCOO–Zr, a significantly greater portion of methoxide species with a Cu weight loading higher than 1.2 wt% were removed from the surface of the catalyst. The apparent first-order rate constant for the removal of methoxide species determined from the initial portion of the transient is given in Table 2. The decrease over the course of the experiment

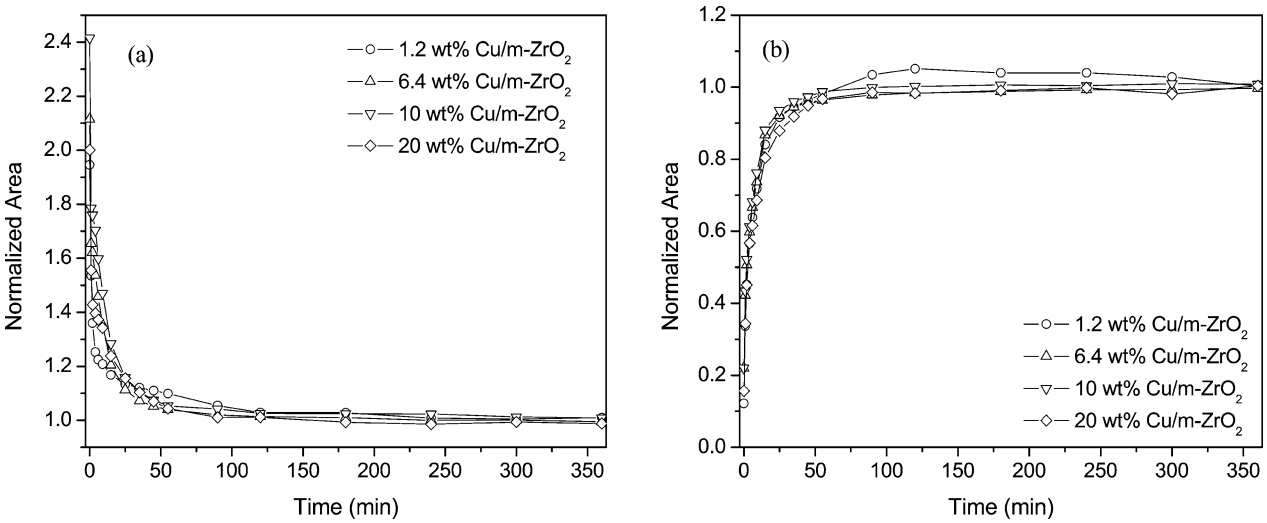


Fig. 10. Relative IR peak intensities of (a) b-HCOO–Zr and (b) $CH_3O$–Zr features for 0, 1.2, 6.4, 10, and 20 wt% Cu/m-$ZrO_2$ during the experiments in Fig. 9. Areas normalized to the values observed at the end of the transient.

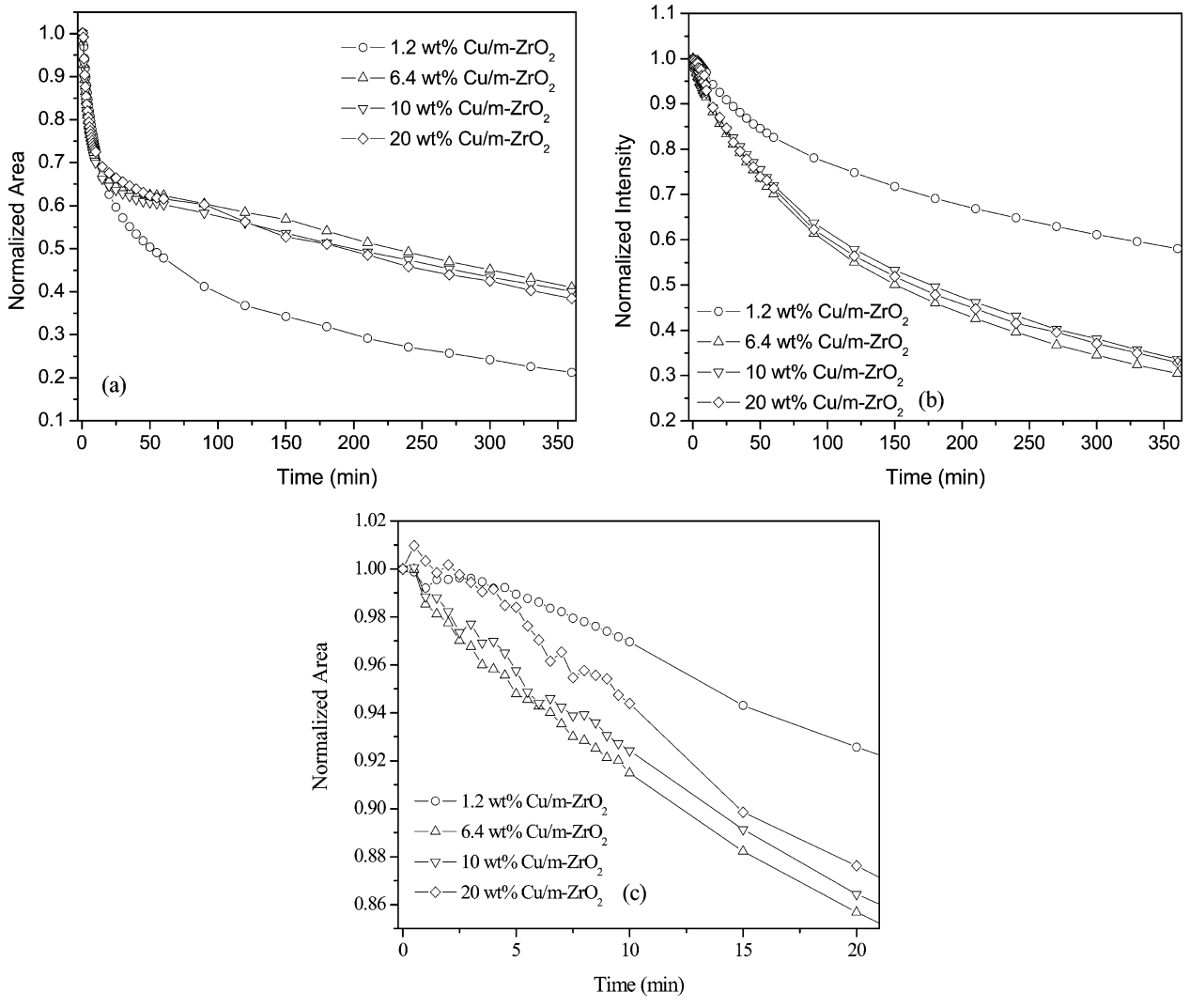


Fig. 11. Relative IR peak intensities of (a) b-HCOO–Zr, (b) $CH_3O$–Zr, and (c) initial 20 min of (b) features for 0, 1.2, 6.4, 10, and 20 wt% Cu/m-$ZrO_2$ at 523 K after switching feed from 0.05 MPa CO, 0.15 MPa $H_2$, and 0.30 MPa He to 0.15 MPa $H_2$ and 0.35 MPa He flowing at a total rate of 60 $cm^3$/min. Areas normalized to the values observed at the beginning of the transient.

was approximately equivalent for 6.4, 10, and 20 wt% Cu/m-$ZrO_2$. Given that b-HCOO–Zr is a precursor to $CH_3O$–Zr on the surface, it is unclear whether the slower relative decrease in methoxide species on 1.2 wt% Cu/m-$ZrO_2$ is a reflection of a higher rate of methoxide group formation through the hydrogenation of b-HCOO–Zr or an inherent difference in the ability to reductively eliminate $CH_3O$–Zr on the surface.

To isolate the inherent dynamics of reductive elimination, $CH_3OH$ was dosed onto both 1.2 wt% Cu/m-$ZrO_2$ and 10 wt% Cu/m-$ZrO_2$ at 523 K. In each case, the catalyst was exposed to a flow containing 0.5% $CH_3OH$/He for 1 h at a total pressure of 0.50 MPa. This process produced $CH_3O$–Zr bands identical to those observed during CO hydrogenation over both catalysts. The $CH_3O$–Zr species produced in this fashion were then exposed to flowing $H_2$ in a manner identical to that used for the experiments presented in Fig. 11. Fig. 12 shows the dynamics of consumption of $CH_3O$–Zr. Peak areas for $CH_3O$–Zr were normalized to the value observed at the beginning of the transient after the removal of physisorbed species ($\sim$ 2 min). For both catalysts the rate of $CH_3O$–Zr hydrogenation is equivalent to that observed after CO hydrogenation (see Fig. 11), and the rate of $CH_3O$–Zr hydrogenation is higher on 10% Cu/m-$ZrO_2$ than on 1.2% Cu/m-$ZrO_2$.

The rate of $CH_3O$–Zr elimination is limited by the concentration of H atoms on the surface of $ZrO_2$, which in turn is limited by the supply of H atoms provided by spillover from Cu. Consistent with this reasoning, it is observed that in the absence of Cu, the rate of $CH_3O$–Zr hydrogenation is an order of magnitude slower than that observed on 1.2% Cu/m-$ZrO_2$. As the surface concentration of Cu is raised, the surface concentration of H atoms increases up to the point at which it reaches equilibrium with respect to the gas-phase partial pressure of $H_2$. When equilibrium is achieved, the rates of H-atom spillover from Cu and reverse spillover back to Cu become identical. The absence of a dependence of the rate of $CH_3O$–Zr hydrogenation on Cu for Cu surface concentration of 1.88 $m^2/g$ suggests that at such Cu surface concentrations, the H-atom concentration on the surface of m-$ZrO_2$ has reached equilibrium with the gas phase.

## 4. Discussion

Previous studies suggest that the mechanism of CO hydrogenation over Cu/$ZrO_2$ catalysts can be described in terms of the following sequence of reactions [9,13]:

$$CO_g + (Zr)_2OH \leftrightarrow \text{b-HCOOZr} + Zr, \quad (1)$$

$$\text{b-HCOOZr} + H_s \rightarrow \cdots \rightarrow CH_3O\text{–Zr} + Zr\text{–OH}, \quad (2)$$

$$CH_3O\text{–Zr} + H_s \rightarrow \rightarrow CH_3OH + (Zr)_2OH. \quad (3)$$

$(Zr)_2OH$ represents a hydroxyl group adjacent to a coordinatively unsaturated Zr cation produced upon creation of an anionic vacancy at the surface of $ZrO_2$ (see Fig. 12 in Ref. [13]). CO is adsorbed reversibly in reaction (1) to form a bidentate formate species (b-HCOOZr). This species then reacts with H atoms present on the surface of $ZrO_2$ ($H_s$), ultimately forming methoxide species ($CH_3O$–Zr) via reaction (2). The reductive elimination of methoxide species in reaction (3) leads to the formation of methanol. Reactions (2) and (3) are taken to be irreversible, since under the reaction conditions used in this study no evidence was found for the dehydrogenation of methoxide or formate species.

As noted earlier, $H_s$ is provided by spillover of H atoms from the dispersed Cu, which adsorbs $H_2$ dissociatively. Investigations of the rate of H/D exchange into hydroxyl groups present on the surface of $ZrO_2$ indicate that at reaction temperature the rate of H atom spillover is about an order of magnitude more rapid than the rate of CO hydrogenation and is significantly faster on Cu/m-$ZrO_2$ than on Cu/t-$ZrO_{e2}$ [12,38]. Studies of methanol decomposition to $H_2$ and $CO_2$ indicate that the decomposition of methanol proceeds on $ZrO_2$ and that dispersed Cu is needed to facilitate the recombination of H atoms [39]. Taken together, these observations suggest that during CO hydrogenation to methanol, the steady-state inventory of H atoms on the surface of $ZrO_2$ is determined by the rates of forward and reverse H-atom spillover and the rate of H-atom consumption for CO hydrogenation. When the rate of CO hydrogenation is slow relative to the rates of forward and reverse spillover, the concentration of $H_s$ will reach an equilibrium level.

The effects of $ZrO_2$ phase on the hydrogenation of CO over 1.2% Cu/t-$ZrO_2$ and 1.2% Cu/m-$ZrO_2$ can now be interpreted in terms of the relative rates of individual steps in the above scheme. Fig. 7 shows that the adsorption of CO on 1.2% Cu/t-$ZrO_2$ is slow, and continues to occur over 6 h, even after $H_2$ has been added to the flow of CO and the hydrogenation of CO has begun. This suggests that the

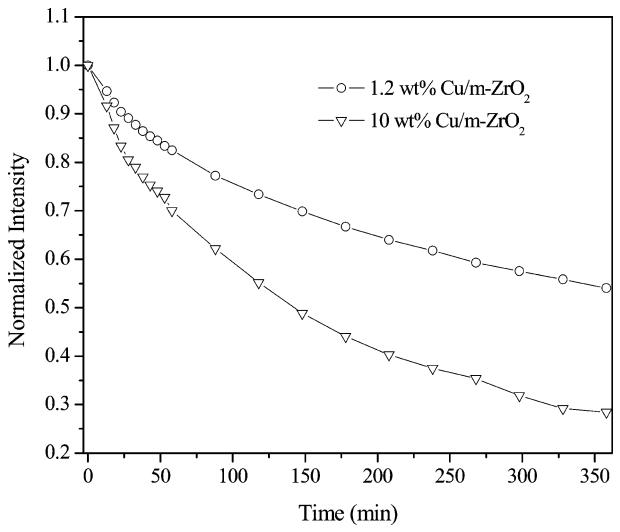


Fig. 12. Relative IR peak intensities of $CH_3O$–Zr features for 1.2 and 10 wt% Cu/m-$ZrO_2$ at 523 K after switching feed from 0.0025 MPa $CH_3OH$ and 0.4975 MPa He to 0.15 MPa $H_2$ and 0.35 MPa He flowing at a total rate of 60 $cm^3$/min. Areas normalized to the values observed at the beginning of the transient.

apparent first-order rate coefficient for reaction (1) is faster than that for reaction (2). In contrast, the rate of CO adsorption on 1.2% Cu/m-$ZrO_2$ is very rapid, and the surface of the catalyst becomes saturated with CO within approximately 1 h (see Fig. 4). When $H_2$ is added to the flow of CO over this catalyst, the surface concentration of b-HCOOZr species decreases rapidly and the surface concentration of $CH_3O$–Zr species increases at the same rate, as seen in Fig. 7. This pattern suggests that the apparent first-order rate coefficient for reaction (2) is faster than that for the reverse of reaction (1). It is also evident from Fig. 7 that the apparent first-order rate coefficient for the formation of $CH_3O$–Zr, determined from the initial slopes of the curves, is a factor of about 2.5 faster for 1.2% Cu/m-$ZrO_2$ than 1.2% Cu/t-$ZrO_2$. A very similar ratio in apparent first-order rate coefficients is seen in Fig. 8 for the reductive elimination of $CH_3O$–Zr as methanol. If it is assumed that the intrinsic rate coefficients for hydrogenation of b-HCOOZr and $CH_3O$–Zr are independent of the phase of $ZrO_2$, then the ratio of apparent rate coefficients suggests that the concentration of $H_s$ is $\sim$ 2.5-fold greater on 1.2% Cu/m-$ZrO_2$. A higher concentration of $H_s$ on Cu/m-$ZrO_2$ relative to Cu/t-$ZrO_2$ would follow from the observation of a higher rate of H-atom spillover (and presumably for reverse spillover) for the former catalyst, as noted above.

The order of magnitude higher rate of methanol synthesis over 1.2% Cu/m-$ZrO_2$ relative to 1.2% Cu/t-$ZrO_2$ can be explained in the following manner. We note first that the concentrations of all carbon-containing species on the former catalyst are higher. Comparison of Figs. 3 and 6 shows that after 6 h of reaction, the surface concentration of b-HCOOZr is $\sim$ 3 times higher on 1.2% Cu/m-$ZrO_2$ than on 1.2% Cu/t-$ZrO_2$, and, more important, the surface concentration of $CH_3O$–Zr is $\sim$ 14 times higher on 1.2% Cu/m-$ZrO_2$. Since the reductive elimination of $CH_3O$–Zr is irreversible under the conditions of the experiments reported here, its rate is equivalent to the rate of methanol synthesis. Researchers reached a similar conclusion in an earlier study by following simultaneously the appearance of the infrared band for $CH_3O$–Zr and the appearance of methanol in the gas phase [9]. Thus one can estimate the relative rates of methanol synthesis on 1.2% Cu/t-$ZrO_2$ and 1.2% Cu/m-$ZrO_2$ by taking the product of the apparent rate coefficient for the reductive elimination of $CH_3O$–Zr and the surface concentration of this species as measured by the intensity of its infrared band (see Table 3). Based on this analysis, it is concluded that the rate of methanol synthesis on 1.2% Cu/m-$ZrO_2$ should be 34 times higher than that on 1.2% Cu/t-$ZrO_2$. Although this factor is greater than the observed 8-fold higher steady-state methanol synthesis activity of 1.2% Cu/m-$ZrO_2$ over 1.2%Cu/t-$ZrO_2$, it supports the idea that the higher rate of methanol synthesis on 1.2% Cu/m-$ZrO_2$ is due largely to the higher concentration of anionic vacancies on the surface of m-$ZrO_2$. These sites facilitate the rapid adsorption of CO.

Table 3
Steady-state peak areas of $CH_3O$–Zr and apparent first-order rate coefficients for the removal of $CH_3O$–Zr from 1.2 wt% Cu/t-$ZrO_2$ and 1.2 wt% Cu/m-$ZrO_2$

| Sample | $k_{app}$ ($min^{-1}$) | $\theta_{CH_3O}$ (a.u.) |
|---|---|---|
| 1.2 wt% Cu/t-$ZrO_2$ | $1.7 \times 10^{-3}$ | 0.9 |
| 1.2 wt% Cu/m-$ZrO_2$ | $4.1 \times 10^{-3}$ | 12.9 |

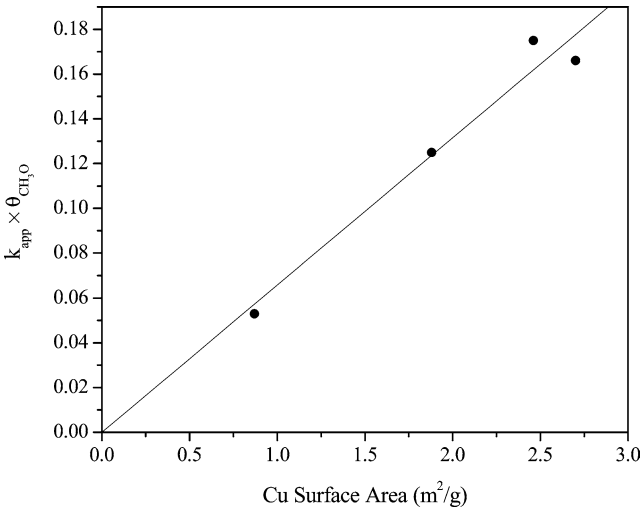


Fig. 13. Product of apparent first-order rate coefficient for $CH_3O$–Zr removal and $CH_3O$–Zr peak area versus Cu surface area for Cu/m-$ZrO_2$ catalysts.

In Part I of this study it was shown that the methanol synthesis activity of Cu/m-$ZrO_2$ catalysts is proportional to the surface area of exposed Cu atoms (see also Table 1). To interpret this observation, it is necessary to consider what happens as the surface concentration of Cu is increased. Table 2 lists the surface concentration of $CH_3O$–Zr and the values of the apparent rate coefficient, $k_{app}$, for the reductive elimination of methoxide groups from the surface of m-$ZrO_2$ as a function of Cu surface area. It is evident that the surface concentration of $CH_3O$–Zr increases with the surface area of Cu up to the level of $\sim$ 2.5 $m^2$/g, whereupon the concentration of $CH_3O$–Zr appears to become constant. The observed variation in the concentration of $CH_3O$–Zr groups is dictated by the balance between the formation and consumption of these species. Since the surface concentration of b-HCOOZr species is essentially independent of the Cu surface area, the increase in the surface concentration of $CH_3O$–Zr is attributed to a higher surface concentration of $H_s$. If it is assumed that reaction (2) is near equilibrium, then one would expect the surface concentration of $ZrOCH_3$ to rise as the surface concentration of $H_s$ increases. The plateau in the surface concentration of $ZrOCH_3$ is attributed to saturation of the $ZrO_2$ surface by $H_s$ when the surface area of Cu is greater than $\sim$ 2.5 $m^2$/g. Table 2 shows that the value of $k_{app}$ also increases with increasing Cu surface area but reaches an apparent plateau above a Cu surface area of

$\sim 1.9\ m^2/g$. Since $k_{app}$ is the product of the intrinsic rate coefficient for reaction 3 and the surface coverage by $H_s$, the approach of $k_{app}$ to a plateau is taken to coincide roughly with the approach of the coverage of $H_s$ to equilibrium. The anticipated effect of Cu surface area on the rate of methanol synthesis can be estimated by taking the product of the surface coverage of $CH_3O$–Zr and $k_{app}$. As seen in Fig. 13, this leads to a linear relationship, which passes through the origin, in good agreement with what is observed from measurements of the rate of methanol synthesis at steady state (see Table 1) [13].

## 5. Conclusions

Formate and methoxide species bound to zirconia are detected by in situ infrared spectroscopy on the surfaces of Cu/t-$ZrO_2$ and Cu/m-$ZrO_2$ during methanol synthesis from CO and $H_2$. The surface concentrations of both species on are an order of magnitude smaller on Cu/t-$ZrO_2$ than on Cu/m-$ZrO_2$. Transient-response experiments suggest that for both catalysts the rate-limiting step in the synthesis of methanol from CO is the reductive elimination of $CH_3O$–Zr species present on the surface of zirconia. The apparent first-order rate coefficient for this process is about 2.5 times higher for Cu/m-$ZrO_2$ than for Cu/t-$ZrO_2$. A major part of this difference is believed to be due to the higher surface concentration of atomic hydrogen on the surface of m-$ZrO_2$ than on t-$ZrO_2$. It is estimated from the product of the coverage of $ZrOCH_3$ and $k_{app}$ that the rate of methanol synthesis should be more than an order of magnitude higher on Cu/m-$ZrO_2$ than on Cu/t-$ZrO_2$, in good qualitative agreement with experimental observation. Both $k_{app}$ and the surface concentration of $CH_3O$–Zr increase with increasing Cu surface area, but reach a plateau. The plateau in each case is attributed to the attainment of an equilibrium concentration in the coverage of the zirconia surface by adsorbed H atoms. The rate of methanol synthesis estimated from the product of $k_{app}$ and the surface coverage of $CH_3O$–Zr versus the Cu surface area yields a linear relationship, in good agreement with the relationship seen between the steady-state rate of methanol synthesis and the Cu surface area.

## Acknowledgment

This work was supported by the Director, Office of Basic Energy Sciences, Chemical Sciences Division of the U.S. Department of Energy, under contract DE-AC03-76SF00098.

## References

[1] B. Denise, R.P.A. Sneeden, Appl. Catal. 28 (1986) 235.
[2] Y. Amenomiya, Appl. Catal. 30 (1987) 57.
[3] Y. Nitta, T. Fujimatsu, Y. Okamoto, T. Imanaka, Catal. Lett. 17 (1993) 157.
[4] Y. Sun, P.A. Sermon, J. Chem. Soc. Commun. 1242 (1993).
[5] D. Bianchi, J.L. Gass, M. Khalfallah, S.J. Teichner, Appl. Catal. 101 (1993) 297.
[6] Y. Nitta, O. Suwata, Y. Ikeda, Y. Okamoto, T. Imanaka, Catal. Lett. 26 (1994) 345.
[7] Y. Sun, P.A. Sermon, Catal. Lett. 29 (1994) 361.
[8] I.A. Fisher, H.C. Woo, A.T. Bell, Catal. Lett. 44 (1997) 11.
[9] I.A. Fisher, A.T. Bell, J. Catal. 172 (1997) 222.
[10] I.A. Fisher, A.T. Bell, J. Catal. 178 (1998) 153.
[11] J. Wambach, A. Baiker, A. Wokaun, Phys. Chem. Chem. Phys. 1 (1999) 5071.
[12] K.T. Jung, A.T. Bell, Catal. Lett. 80 (2002) 63.
[13] M.D. Rhodes, A.T. Bell, J. Catal. 233 (2005) 198.
[14] S. Sato, R. Takahashi, T. Sodesawa, K. Yuma, Y. Obata, J. Catal. 196 (2000) 195.
[15] R.F. Hicks, C.S. Kellner, B.J. Savatsky, W.C. Hecker, A.T. Bell, J. Catal. 71 (1981) 216.
[16] C. Schild, A. Wokaun, A. Baiker, J. Mol. Catal. 63 (1990) 243.
[17] M.Y. He, J.G. Ekerdt, J. Catal. 87 (1984) 381.
[18] J. Kondo, H. Abe, Y. Sakata, K. Maruya, K. Domen, T. Onishi, J. Chem. Soc. Faraday Trans. 1 84 (1988) 511.
[19] W. Hertl, Langmuir 5 (1989) 96.
[20] E. Guglielminotti, Langmuir 6 (1990) 1455.
[21] D. Bianchi, T. Chafik, M. Khalfallah, S.J. Teichner, Appl. Catal. A: Gen. 105 (1993) 223.
[22] H. Kalies, N. Pinto, G.M. Pajonk, D. Bianchi, Appl. Catal. A: Gen. 202 (2000) 197.
[23] K. Pokrovski, K.T. Jung, A.T. Bell, Langmuir 17 (2001) 4297.
[24] J. Edwards, G. Schrader, J. Phys. Chem. 89 (1985) 782.
[25] D. Bianchi, T. Chafik, M. Khalfallah, S.J. Teichner, Appl. Catal. A: Gen. 112 (1994) 57.
[26] K.D. Jung, A.T. Bell, J. Catal. 193 (2000) 207.
[27] Y. Okamoto, H. Gotoh, Catal. Today 36 (1997) 71.
[28] Y. Okamota, H. Gotoh, H. Aritani, T. Tanaka, S. Yoshida, J. Chem. Soc. Faraday Trans. 93 (1997) 3879.
[29] V. Indovina, M. Occhiuzzi, D. Pietrogiacomi, S. Tuti, J. Phys. Chem. B 103 (1999) 9967.
[30] J. Erkelens, H.Th. Rijnten, S.H. Eggink-Du Burck, Recueil 91 (1972) 1426.
[31] A. Trunschke, D.L. Hoang, H. Lieske, J. Chem. Soc. Faraday Trans. 91 (1995) 4441.
[32] J. Weigel, R.A. Koeppel, A. Baiker, A. Wokaun, Langmuir 12 (1996) 5319.
[33] M. Bensitel, V. Moravek, J. Lamonte, O. Saur, J.C. Lavalley, Spectrochim. Acta 43a (1987) 1487.
[34] D. Bianchi, T. Chafik, M. Khalfallah, S.J. Teichner, Appl. Catal. A: Gen. 123 (1995) 89.
[35] F. Ouyang, J.N. Kondo, K. Maruya, K. Domen, J. Phys. Chem. B 101 (1997) 4867.
[36] F. Ouyang, J.N. Kondo, K. Maruya, K. Domen, Catal. Lett. 50 (1998) 179.
[37] J. Saussey, J.C. Lavalley, J. Mol. Catal. 50 (1989) 343.
[38] K.D. Jung, Bell, J. Catal. 193 (2000) 207.
[39] I.A. Fisher, A.T. Bell, J. Catal. 184 (1999) 357.